EARTH SURFACE PROCESSES AND LANDFORMS
Earth Surf. Process. Landforms **43**, 218–228 (2018)

Published online 4 October 2017 in Wiley Online Library
(wileyonlinelibrary.com) DOI: 10.1002/esp.4234

Hydrogeomorphological differentiation between floodplains and terraces

Qina Yan,[1] Toshiki Iwasaki,[2] Andrew Stumpf,[3] Patrick Belmont,[4] Gary Parker[1,5] and Praveen Kumar[1,6]*
[1] Department of Civil and Environmental Engineering, University of Illinois, Urbana, IL 61801, USA
[2] Civil Engineering Research Institute for Cold Region, Hokkaido, Japan
[3] Illinois State Geological Survey, Prairie Research Institute, University of Illinois, Champaign, IL 61820, USA
[4] Department of Watershed Sciences, Utah State University, Logan, UT 84322, USA
[5] Department of Geology, University of Illinois, Urbana, IL 61801, USA
[6] Department of Atmospheric Sciences, University of Illinois, Urbana, IL 61801, USA

Received 1 February 2017; Revised 16 August 2017; Accepted 17 August 2017

*Correspondence to: Praveen Kumar, Department of Civil and Environmental Engineering, University of Illinois, Urbana, IL 61801, USA. E-mail: kumar1@illinois.edu

ESPL
Earth Surface Processes and Landforms

ABSTRACT: Floodplains and terraces in river valleys play important roles in the transport dynamics of water and sediment. While flat areas in river valleys can be identified from LiDAR data, directly characterizing them as either floodplain or terraces is not yet possible. To address this challenge, we hypothesize that, since geomorphic features are strongly coupled to hydrological and hydraulic dynamics and their associated variability, there exists a return frequency, or possibly a narrow band of return frequencies, of flow that is associated with floodplain formation; and this association can provide a distinctive signature for distinguishing them from terraces. Based on this hypothesis we develop a novel approach for distinguishing between floodplains and terraces that involves transforming the transverse cross-sectional geometry of a river valley into a curve, named a river valley hypsometric (RVH) curve, and linking hydraulic inundation frequency with the features of this curve. Our approach establishes that the demarcation between floodplains and terraces can be established from the structure of steps and risers in the RVH curves which can be obtained from the DEM data. Further, it shows that these transitions may themselves be shaped by floods with 10- to 100-year recurrence. We additionally show that, when floodplain width and height (above channel bottom) are normalized by bankfull width and depth, the ratio lies in a narrow range independent of the scale of the river valley. Copyright © 2017 John Wiley & Sons, Ltd.

KEYWORDS: river valley; hydrogeomorphology; flood simulation; floodplain and terrace

Introduction

Floodplains, terraces, meanders, levees, bars and other features that are present within river valleys provide valuable insights into the geomorphic and hydrological legacies that shape them (Bridge, 2003). Each of these features plays a role in river morphology, and they are important determinants of space–time variability of water and sediment flux (Bull, 1990; Bridge, 2003; Pazzaglia, 2013). Further, these features shape the dynamic interaction between river flows and the riparian corridor through hydrological exchange of fluxes, which impacts their biogeochemical and ecological functions (Corenblit *et al.*, 2011; Harvey and Gooseff, 2015).

Among the various geomorphic features, floodplains and terraces together cover a significant part of a river valley. Floodplains are areas that are adjacent to the river and formed by the river in its current hydrological regime and are inundated at times of high water (Leopold et al., 1964; William Dietrich, personal communication, April 2017). Terraces are former and abandoned floodplains that are not well integrated into the existing hydrological regime of the river (Pazzaglia and Gardner, 1993). Terraces and floodplains have long been utilized for agriculture and urban development because of their relatively flat surfaces and proximity to rivers. The landforms and underlying alluvial deposits of terraces record long-term geomorphic and hydrological responses to climatic and tectonic history (Bull, 1990; Hancock and Anderson, 2002; Pazzaglia, 2013). Floodplains and terraces play important and distinct roles in terms of channel migration, channel width adjustment and sediment source-to-sink dynamics (Bull, 1990; Nanson and Croke, 1992; Bridge, 2003; Belmont, 2011; Gran *et al.*, 2013; Pazzaglia, 2013; Stout and Belmont, 2014). Therefore, extracting and classifying these features from elevation data and establishing the dynamical basis of their formation are important for developing deeper insight for both predictive and phenomenological modeling (Kumar, 2011), with potential applications in managing sediment budgets, designing stream restoration schemes, and evaluating flood risks (Arthington and Pusey, 2003; Opperman *et al.*, 2009).

Identifying and distinguishing between terraces and floodplains are long-standing questions in geomorphological studies. Traditionally, identification of floodplains in a river valley is based on either historical flood hazard mapping or hydraulic modeling with field surveys (Noman *et al.*, 2001; Degiorgis *et al.*, 2012; Grimaldi *et al.*, 2013; Wyrick *et al.*, 2014; Wheaton *et al.*, 2015). In this work, we hypothesize

that, since geomorphic features are strongly coupled to hydrological and hydraulic dynamics and their associated variability, there exists a return frequency, or possibly a narrow band of return frequencies, of flow that is associated with floodplain formation; and this association can provide a distinctive signature for distinguishing them from terraces. This hypothesis is in part inspired by and an extension of the empirical observation that bankfull geometry of stream channels, in a range of geological and climatic settings, is strongly associated with 1- to 2-year return flows (Leopold *et al.*, 1964). Hydraulic geometry at the channel scale has been the subject of much investigation (Park, 1977; Rhodes, 1977; Williams, 1978; Knighton, 1998; Bridge, 2003; Dodov, 2004), but hydraulic geometry at the river valley scale has not been adequately characterized, although important contributions have been made (Leopold *et al.*, 1964; Bhowmik and Stall, 1979; Bridge, 2003).

Methods have been developed (Degiorgis *et al.*, 2012; Stout and Belmont, 2014) to identify 'flat' areas from high-resolution LiDAR (light detection and ranging) digital elevation model (DEM) data (Passalacqua *et al.*, 2015), which may potentially be categorized as a floodplain or terrace. However, little is known about the magnitude and return frequencies of flows that shape floodplains, and how we may distinguish them from terraces directly from DEM data. Existing approaches based on the geometric features of these flat areas, such as elevations and slopes, are inadequate (Hopkins and Snyder, 2016). Our hypothesis serves as a basis for addressing these two questions simultaneously.

In this paper, we propose a new approach for defining and distinguishing between terraces and floodplains. It involves transforming the transverse cross-sectional geometry of a river valley into a curve, named a river valley hypsometric (RVH) curve, and linking hydraulic inundation frequency with the features of this curve. We develop and test the proposed method using data from eight river valley reaches within three representative watersheds in the Upper Mississippi River Basin (Figure 1). These study sites are within the Critical Zone Observatory for Intensively Managed Landscapes (http://www.imlczo.org). These river valleys were shaped by Pleistocene ice sheets, but they have since evolved through different evolutionary pathways. The method is further verified using data from eight other Critical Zone Observatory sites. We first present the basic concept of characterizing the cross-sectional geometry of a river valley in terms of a RVH curve. Second, we compare the topographic characteristics among the eight river valley reaches (within the Upper Mississippi River basin) based on their RVH curves and then propose a delineation of the channel–floodplain zone in a river valley to distinguish them from the terraces. Third, we run 2D flood simulations to evaluate the assumed delineation. Last, we investigate the hydro-geomorphological features that alluvial river valleys have in common, and compare across other non-alluvial sites.

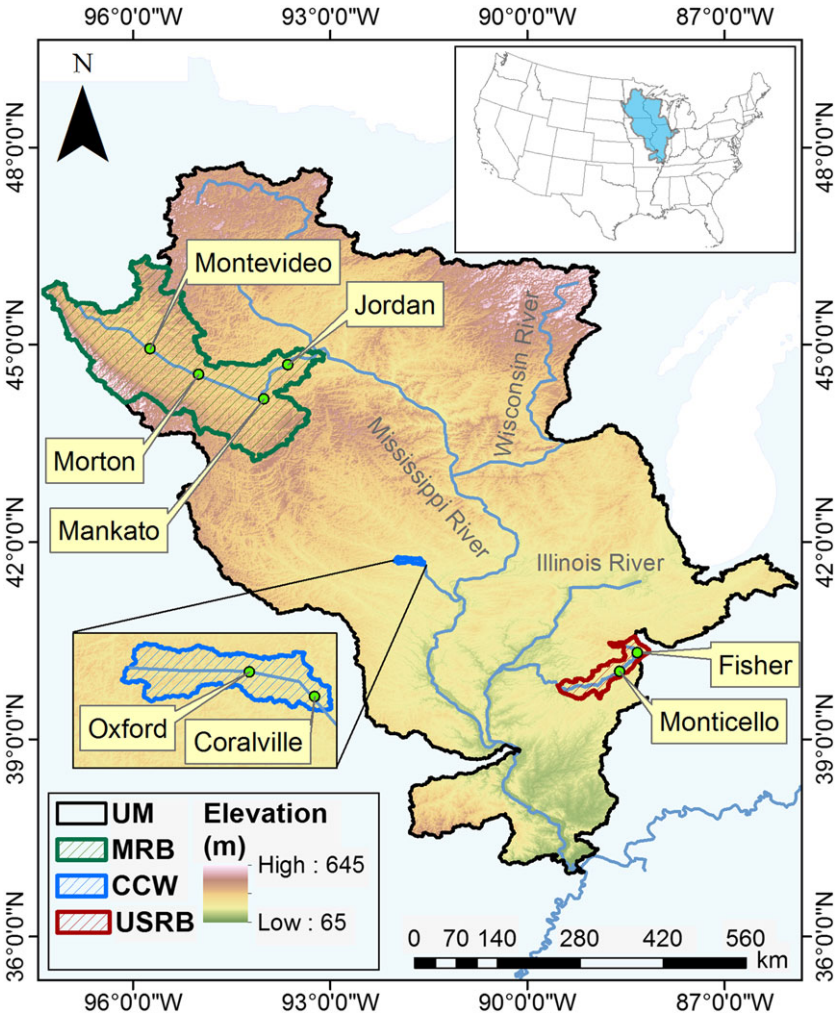

Figure 1. Map of Upper Mississippi (UM) River Basin, which includes the study sites in the Minnesota River Basin (MRB), the Clear Creek Watershed (CCW) and the Upper Sangamon River Basin (USRB). Locations labeled with circles are USGS stream gaging stations. [Colour figure can be viewed at wileyonlinelibrary.com]

Study sites

Our primary study sites include three river valleys in the Upper Mississippi River Basin (Figure 1). The sites are in the Clear Creek Watershed (CCW) in Iowa, the Upper Sangamon River Basin (USRB) in Illinois and the Minnesota River Basin (MRB) in Minnesota. This region was glaciated multiple times during the Pleistocene Epoch (2.6 million to 11 700 years ago; Fan and Hou, 2016). These glaciations include several major continental advances of the Laurentide Ice Sheet that had both regional and local impacts (Mickelson and Colgan, 2003). The glaciers deeply buried the bedrock in stratified sediment and till, and the average thickness of glacial deposits is estimated to have been between 40 and 100 m across the three watersheds (Soller *et al.*, 2012). Some parts of the region, including the MRB and the USRB, were glaciated during the Late Pleistocene (12 000–30 000 years ago; Killey, 2007; Jennings and Johnson, 2011; Cohen and Gibbard, 2016). These watersheds tend to have poorly integrated natural drainage networks with low-gradient, shallow water tables, and relatively thin weathering profiles (Patterson *et al.*, 2003). Other parts of the Midwest, including the CCW, were last glaciated during the Early to Middle Pleistocene (130 000–2 580 000 years ago; Killey, 2007; Rovey and Balco, 2015). Because of this, the CCW has better integrated drainage networks, a wider range of gradients and thicker weathering profiles (Rovey and McLouth, 2015).

The USRB, MRB, and CCW represent a range of typical land uses, soil properties and stream network configurations in the Upper Midwest, and each site has unique hydrological and geomorphic characteristics. The 3690 km^2 USRB is a well-studied river system. Analysis of aerial photos, taken by the US Department of Agriculture (USDA) from 1940 to 2015, indicates that the course of the Sangamon River has shown negligible migration and the river width has barely changed (Rhoads *et al.*, 2016). This suggests that the river system is close to a quasi-equilibrium condition and that the resistance of the alluvial sediments is equal to or greater than erosional forces. In contrast, major tributaries within the 44 000 km^2 MRB are undergoing exceptionally rapid incision in response to a base-level fall (Belmont *et al.*, 2011; Belmont, 2011; Gran *et al.*, 2013) as well as increased river discharges because of land cover change for agriculture (Foufoula-Georgiou *et al.*, 2015). The mainstem Minnesota River, scoured by a catastrophic glacial outwash event 13 400 years ago, is rapidly aggrading (Wilcock, 2009). The CCW covers 270 km^2 in east-central Iowa. Many studies of this watershed show that agricultural practices have enhanced the rate of soil erosion on highly erodible soils in both uplands and river valleys, resulting in increasingly high sediment delivery and higher storm flow peaks (Abaci and Papanicolaou, 2009; Rayburn and Schulte, 2009; Wilson *et al.*, 2009).

We used the TerEx toolbox (Stout and Belmont, 2014) to identify and map polygons corresponding to flat areas as candidates for being categorized as floodplains or terraces, and

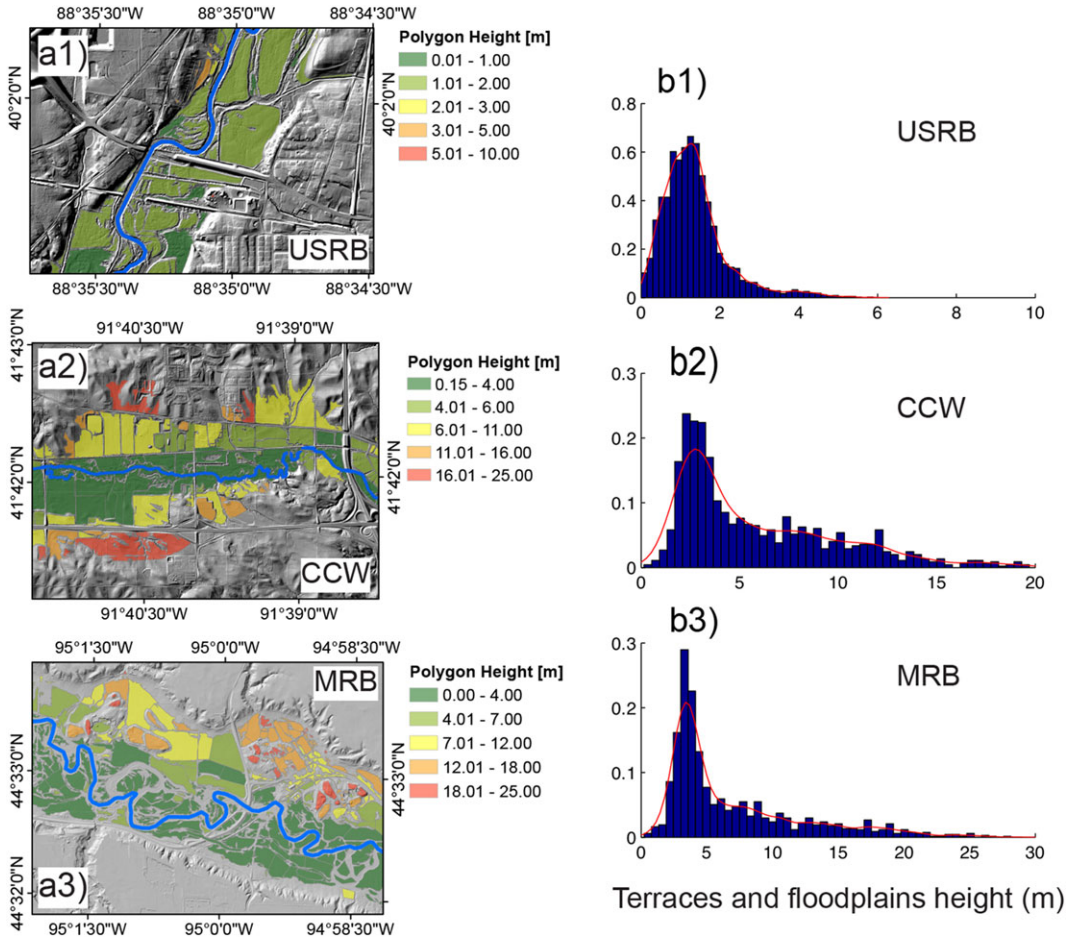

Figure 2. Mapping and statistical analysis of the relatively flat areas as candidates for terraces and floodplains in USRB, CCW and MRB. (a1–a3) An illustrative example in USRB, CCW and MRB respectively. The colored areas are identified flat areas in the river valley based on TerEx toolbox (Stout and Belmont, 2014). The numbers on the upper right insert represent the heights (from the channel elevation) in meters. The mapped valley reach covers two USGS gaging stations, Fisher and Monticello. (b) Probability density functions (PDFs) of the heights of the flat areas for the USRB, CCW and MRB, respectively. The red solid lines are approximate PDF curves. [Colour figure can be viewed at wileyonlinelibrary.com]

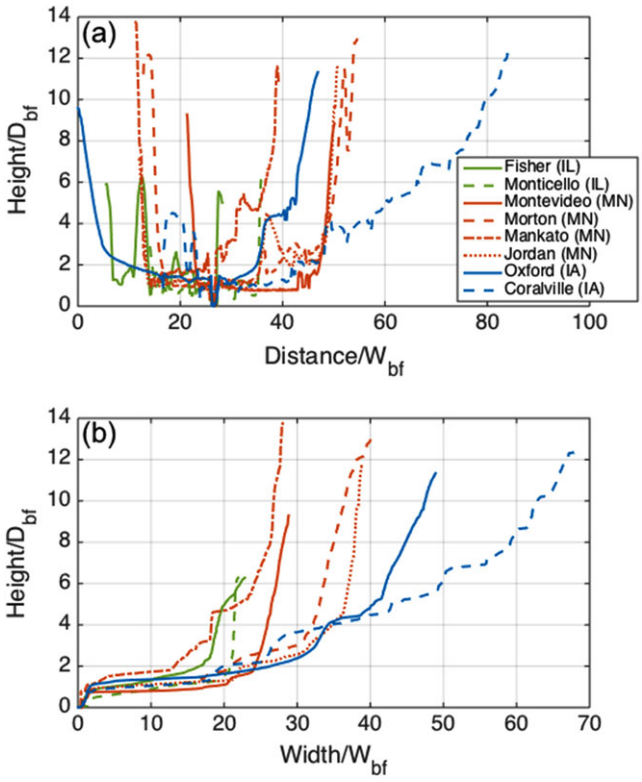

Figure 3. Illustration of cross-sections of river valley topographies and RVH curves for the eight study sites in Intensively Managed Landscapes (IML). (a) Normalized cross-sectional geometries of river valleys. (b) The corresponding normalized RVH curves. [Colour figure can be viewed at wileyonlinelibrary.com]

extract their area and height (defined as the relative vertical distance to the nearest river bed) from a LiDAR DEM. We used a 1.2 m LiDAR DEM for the USRB (from the Illinois State Geological Survey (ISGS)) and 1.0 m LiDAR DEM for both the MRB (from the Minnesota Geospatial Database) and CCW (from the National Topography Database). Since floodplains have lower height differentials with the local channel as compared to terraces, extracting the heights of the relatively flat polygonal areas in river valleys could potentially reveal the vertical distance gap between terraces and floodplains. The highlighted polygons in the spatial maps, shown in Figure 2(a1–a3), are illustrative examples from the three watersheds. Mapped valley reaches cover two USGS gaging stations in each watershed: Fisher and Monticello in the USRB, Oxford and Coralville in the CCW, and Morton and Mankato in the MRB (Figure 1). The probability density functions (PDFs) are shown in Figure 2(b1–b3). The PDF for USRB shows that the heights lie in a narrow range, and in addition the PDF does not have a long tail, which suggests that this valley reach includes predominantly floodplains. In contrast, the PDFs in CCW and MRB show a long-tail distribution, which indicates that there could be both terraces and floodplains in the valley reach. Even though we are able to capture the heights of flat areas from LiDAR DEMs, there remains ambiguity with regard to which specific surface should be classified as a terrace or floodplain. Next we introduce a relatively simple but novel framework that can play a useful role in this categorization.

River Valley Hypsometric Curve

The concept of the hypsometric curve was first introduced by Strahler (1952) to quantify, in a general way, the geomorphological features of watersheds. In its original form, it displays the area that lies above a specified elevation, by plotting elevation on the ordinate and the area above that elevation on the abscissa. Here we adopt a similar concept to describe the shape of river valleys. Our approach is based on transforming the cross-sectional geometry of a river valley into a relation between the height, defined as the elevation above the river bottom, and the width, defined as the corresponding horizontal span. With increasing height, the width generally increases. Flat areas, like floodplains and terraces, have very small local relief, so a small increase in height corresponds to a large increase in the lateral span. We define this height–width relationship as a river valley hypsometric (RVH) curve. To enable comparison across valleys of differing scales, we normalize the height and width with bankfull depth, D_{bf}, and width, W_{bf}, respectively. Low-gradient segments (here referred to as steps) in the RVH curve represent flat areas in the river valley. In contrast, steep segments (here referred to as walls or 'risers') represent zones of steep slope in the cross-section. In general, gradients in the RVH curve match the slopes from the cross-sectional geometry of the river valley.

Eight valley reaches (four in MRB, two in USRB and two in CCW; Figure 1) were selected for analysis to demonstrate the information that can be extracted from RVH curves. Each reach is about 1 km long and immediately downstream from a gaging station. Cross-sectional lines were generated orthogonal to the longitudinal direction of the valley at 2 m intervals. To obtain a representative cross-section for the entire valley reach, the river bottoms of all cross-sections were overlaid on top of each other and elevations were averaged. Figure 3a shows the averaged cross-sectional lines thus obtained for the eight river valley reaches. The corresponding RVH curves are shown in Figure 3b. For normalizing, we use channel bankfull width and depth data from the USGS (US Geological Survey field measurements, data accessed June 2016). Supporting Information Table S1 provides details related to the study sites' river and river valley geometries.

Based on the general features of the RVH curves, we can classify the transverse cross-sectional forms of the river valleys in our study area into three categories: V-shape, U-shape and U-shape with terraces (henceforth UT-shape) (Figure 4a1–a3). The shapes of the river valley imply a sediment mass balance that ranges from net-incisional to net-aggradational (Nanson and Croke, 1992; Schumm, 2005; Limaye and Lamb, 2014). A V-shape valley (Figure 4b1) is relatively narrow compared to the other two valley types, suggesting active incision. Flat floodplains are relatively narrow or absent in this type of valley. A U-shape valley (Figure 4b2) is a flat-bottomed valley, indicating that the valley wall is widening and/or the valley bottom is undergoing aggradation. A UT-shape valley (Figure 4b3) is a flat-bottomed valley with terraces, indicating that there have been former high river levels whose geomorphic signatures are preserved. In some cases, the terraces may be strath terraces if the valley widens as the river has incised over time. In other cases these may be alluvial fill terraces if the river aggraded and has incised back through its alluvial deposits.

For the study sites, the RVH curves (Figure 3b) show different levels of flat segments much more clearly than the cross-sectional lines themselves (Figure 3a). For example, the river valley in Fisher is close to a V-shape valley, whereas Monticello resembles a U-shape valley. There is only one step (or low-gradient segment) on the RVH curves of the two USRB sites. This means that all flat areas may be floodplains rather than terraces. The four valley reaches in the MRB (Montevideo, Morton, Mankato and Jordan) resemble U-shape and UT-shape valleys. Higher sediment loading from rapidly

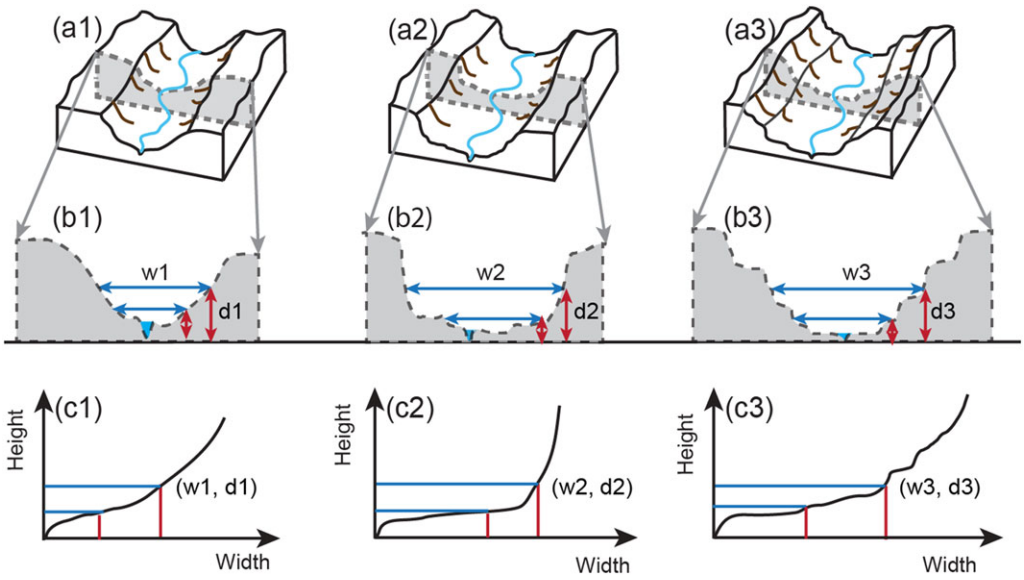

Figure 4. Illustration of different river valley shapes. (a) Schematics of different types of river valleys (from left to right): V-shape, U-shape and UT-shape (U-shape with terraces). (b) Illustration of the corresponding cross-sectional geometries extracted from (a). (b1) V-shape valley: the floodplain is relatively narrow or absent, and the channel is experiencing active incision at this stage. (b2) U-shape valley: the floodplain has clear flat zones, and the system may be at or near grade. (b3) UT-shape valley: it has both floodplain and terraces, and hence there is more than one flat level in the river valley. The floodplain may be actively aggrading at this stage. (c) The corresponding river valley hypsometric (RVH) curves. [Colour figure can be viewed at wileyonlinelibrary.com]

incising tributaries (Belmont *et al.*, 2011) causes active aggradation in the mainstem of the Minnesota River (Wilcock, 2009; Li, 2014), which can drive rapid channel migration rates as well as frequent cutoffs. The RVH curves at the two sites in the CCW (Oxford and Coralville) also resemble UT-shape valleys, but they have larger scales in both non-dimensional width and depth. The presence of more risers (which link the lowermost and second lowermost low-gradient segments on the RVH curve) support the hypothesis that the CCW could have more terraces than the other two watersheds. One unusual curve in Figure 3 is Mankato, which is located in an urbanized area and includes a large concrete flood control structure.

It is of interest to note from Figure 3b that, while actual valley widths vary (see Supporting Information Table S1), all of the curves more or less collapse into a range (width/W_{bf}, height/D_{bf}) $\leq$ (18, 1.5). The point (width/W_{bf}, height/D_{bf}) = (18, 1.5) is near the end of the lowermost low-gradient segment on the RVH curve for all valley reaches. Hence the zone for which (width/W_{bf}, height/D_{bf}) falls within (18, 1.5) can be used to loosely define the floodplain. In the following sections, we will run 2D flooding simulations to test this proposition and define the floodplain in greater detail.

Flood Simulation

Discharge estimation

Daily data of discharge and stage height from gaging stations are available from the USGS (http://waterdata.usgs.gov/nwis/rt). Bankfull discharge is defined as the stage at which streamflow starts to inundate floodplains. We estimated the bankfull discharge using the break in slope of the stage–discharge relations (Figure 5a) recorded at the USGS gaging stations (Leopold and Maddock, 1953; Williams, 1978). Here 'stage' refers to water surface height from a constant base level that is lower than the river bottom. Once the flow overtops the river bank, stage increases more gradually with discharge due to the storage available in the

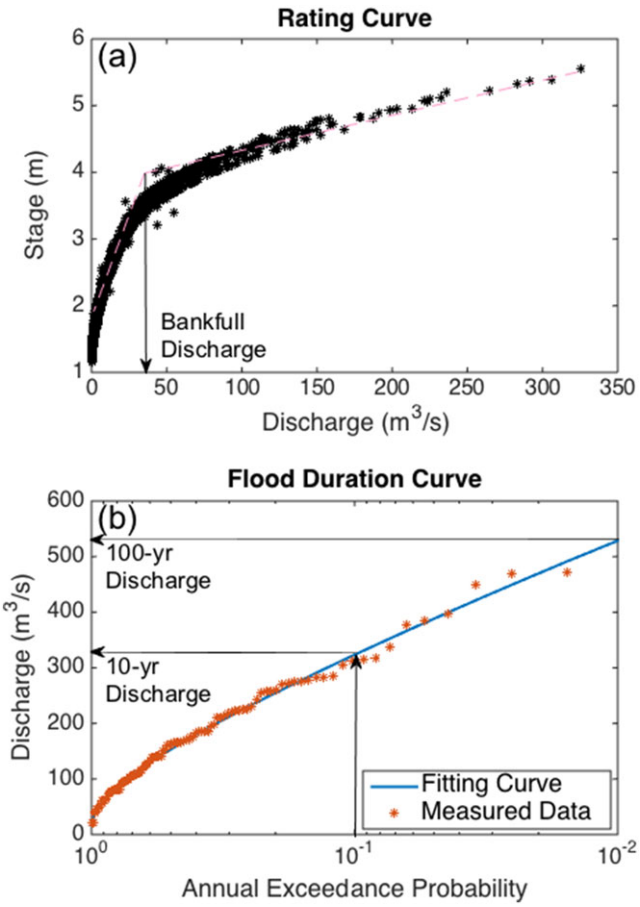

Figure 5. Illustration of the determination of bankfull discharge, and 10- and 100-year discharges in Monticello, USRB. (a) Bankfull discharge estimation. Discharge and stage data correspond to daily records from USGS gaging station (http://waterdata.usgs.gov/nwis/rt). (b) 10- and 100-year discharge estimation. Annual maximum discharges are from the same USGS gaging station. The fitted curve is based on a combination of the log-Pearson type III distribution and empirical regional equations adopted by USGS. [Colour figure can be viewed at wileyonlinelibrary.com]

floodplain, which results in a lower slope in the stage–discharge relation. The transition point on the curve is regarded as the bankfull condition (Figure 5a). We analyzed data from two stations in USRB (Fisher and Monticello), four stations in MRB (Montevideo, Morton, Mankato, Jordan), and two stations in CCW (Oxford and Coralville). The bankfull discharges are summarized in Supporting Information Table S2.

In order to consider a range of return periods of floods to link to floodplain and terrace delineation, we use three typical hydrological scenarios. These are bankfull discharge, and 10-year and 100-year return periods. As indicated from results in the next section, these three scenarios capture the range of variability of inundation needed for the study. 10-year and 100-year discharges were estimated based on the log-Pearson Type III distribution, which serves as a default distribution for flood frequency analysis, and then modified by regional empirical equations according to USGS technical reports (Soong *et al.*, 2004; Lorenz *et al.*, 2010; Eash *et al.*, 2013). Annual maximum discharge records are also available from the USGS database. To estimate the flood return periods, we assumed stationarity and used the entire record. Figure 5b shows an example of a curve fit to the observed annual maximum discharges at the Monticello gaging station.

A correction to discharge input is needed before using LiDAR DEM to simulate flooding. This correction accounts for the fact that the near-infrared LiDAR that is used to create the DEM usually does not fully penetrate water bodies. Penetration depth depends on water clarity or turbidity. We compared LiDAR DEM with ADCP (acoustic Doppler current profiler) field measurements, and found that, even though the LiDAR data were obtained during low flow conditions, the stream bed represented in the DEM lies between the water surface and the actual stream bed. As a result, the 'false' river bottom in the LiDAR DEM already accounts for a certain amount of flow within the streams. This requires a correction before implementing the hydrodynamic calculation. Here we make the assumption that the flow discharge at the time the LiDAR data were acquired was low compared to bankfull or higher flood discharges. We estimated this discharge Q_{lidar} from the observed 'false' river bottom from the LiDAR data and the relevant rating curve for the site. In running the hydrodynamic model at bankfull discharge Q_{bf}, the discharge we used in the model is $Q_{bf} - Q_{lidar}$. We use the same procedure for the higher discharges, i.e. the 10-year and 100-year floods. Supporting Information Table S2 summarizes bankfull, 10-year and 100-year discharges, as well as Q_{lidar} corresponding to the 'false' river bottom for all gaging sites. As can be seen from Table S2, estimated Q_{lidar} is indeed much smaller than any of the relevant flood discharges, justifying the rationale behind the above adjustment.

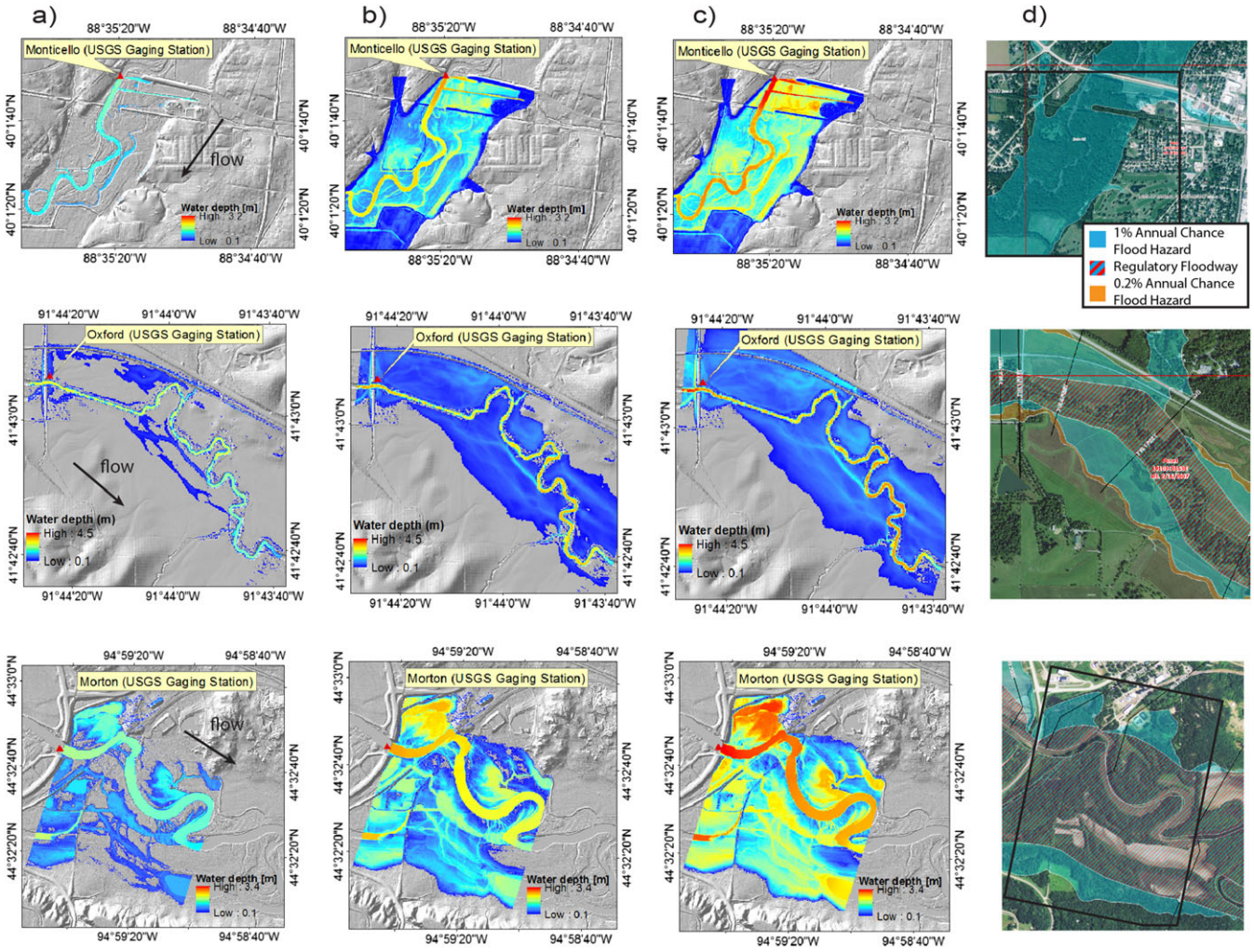

Figure 6. Illustration of flood simulation results at three sites: Monticello (top), Oxford (middle) and Morton (bottom). (a), (b) and (c) show water depth for bankfull discharge, and 10- and 100-year flood, respectively. (d) Flooding area of 100-year flood from FEMA's National Flood Hazard Layer digital database. The solid boxes in (d) cover the same areas as (a), (b) and (c). [Colour figure can be viewed at wileyonlinelibrary.com]

Model and results

We used the Nays2D Flood model to simulate flooding events. The tool is open source and a part of the International River Interface Cooperative (iRIC) software package. The iRIC package was developed in collaboration with the USGS and the Foundation of the Hokkaido River Disaster Prevention Research Center (Nelson *et al.*, 2016). The Nays2D Flood model uses a 2D shallow-water flow formulation, which is solved with a finite difference scheme. This model has been applied extensively, with examples including a severe flood event in Thailand that occurred in 2011 (Wongsa, 2014) and a sediment transport study in the Abukuma River floodplain related to the Fukushima nuclear disaster (Iwasaki *et al.*, 2014).

We simulated bankfull, and 10-year and 100-year recurrence flows to explore the relationship between the occurrence of large floods and geomorphic features in our selected river valleys. At each of the sites, flows were simulated for a constant discharge for reach segments where no tributaries join the main stem. To investigate the highest possible water level for a flood of a specified recurrence, the duration of the simulation was sufficiently long to allow the outflow to reach steady state with the inflow. In this model, infiltration into the ground was ignored. The Manning roughness coefficient, another important parameter, was calibrated with observed water level at each gage station. We first assumed a spatially uniform roughness coefficient across the channel and floodplain in the model, and then calibrated based on the difference in water surface level from a gaging station with the one predicted from the simulation. After calibration, the Manning roughness coefficient was found to be approximately 0.03 for all eight study sites. This value is reasonable for sand-bed channels and floodplains with low to moderate vegetation (Chow *et al.*, 1988).

Figure 6a–c illustrates the flow simulations for three sites, Fisher, Oxford and Mankato, with water depths shown at bankfull discharge, and 10-year and 100-year flood respectively. We observe that bankfull discharge may not be completely confined within a river channel. Due to the uneven heights of river banks over the length of its reach, zones near the channel can also be inundated to some degree. The 10-year flood results in less inundation area and shallower water depth compared to the 100-year flood, as expected, but the differences are not significant (see next section for statistical comparison). Figure 6d shows the map of flooding area of the 100-year flood from FEMA's National Flood Hazard Layer (NFHL) digital database (https://fema.maps.arcgis.com). The Nays2D Flood model provides similar results (Figure 6c) to those in the NFHL database. In the next section we use the simulated results to investigate the relationship between flood water level and the RVH curve.

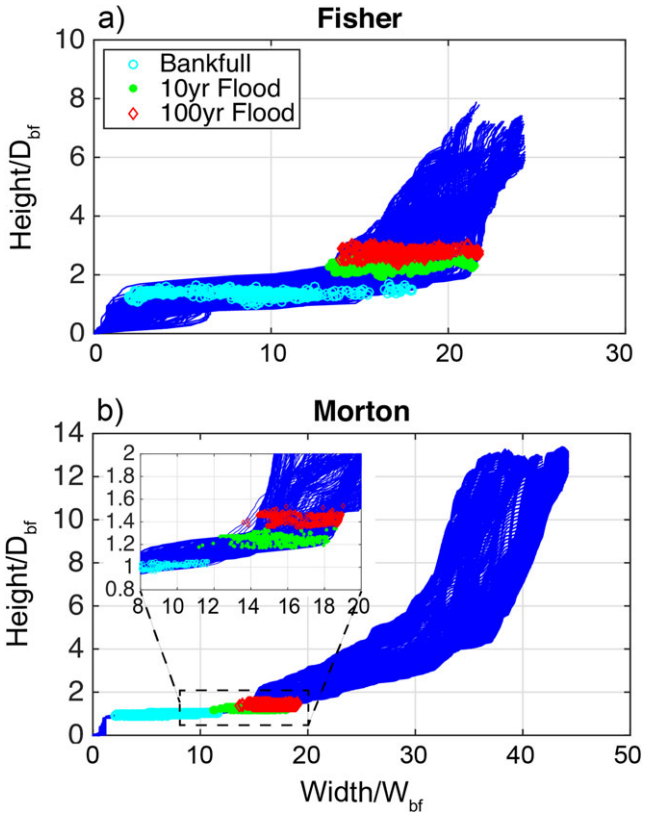

Figure 7. Illustration of water levels overlain on normalized RVH curves (all of the eight sites are shown in Supporting Information Figure S1). Valley height and width are normalized by bankfull depth D_{bf} and bankfull width W_{bf}, respectively. The normalized RVH curves have been extracted longitudinally along each river valley reach at 2 m intervals. Locations of the three discharges on the curves are represented as symbols in the RVH curves; the open cyan circles represent bankfull discharge, the closed green circles represent the 10-year flood and open red diamonds represent to the 100-year flood. [Colour figure can be viewed at wileyonlinelibrary.com]

Distinguishing Terraces and Floodplains

To verify the hypothesis that there is a formative relationship between recurrence frequency of floods and floodplain cross-sectional geometry, we plot the simulated water heights and surface widths on the corresponding RVH curves (Figure 7) under the three flow discharges (bankfull, and 10-year and 100-year recurrence). Each cross-section has an RVH curve, and every valley reach has abundant cross-sectional lines. On each RVH curve, we mark the three discharge scenarios as open circles for bankfull discharge, closed circles for 10-year flood and open diamonds for 100-year floods.

From this figure, we see that bankfull discharge is barely at the lowermost step on the RVH curve. Both 10-year and 100-year floods are blocked by the riser in the curve. Although there is no precise threshold between floodplain and terrace, the present results suggest that the lowermost step on the RVH curve designates a floodplain, and the steps above are terraces. The results of all eight sites in the USRB, MRB and CCW are shown in Supporting Information Figure S1. We note from this figure that water surface elevation at the 100-year flood provides a reasonable threshold for separating terraces from floodplains. At most of the sites (except for Mankato), the water surface elevation at the 10-year flood provides results that are very close to the 100-year flood. At Fisher, Monticello and Montevideo (Figure S1), there is only one step on each RVH curves, so we conclude that there are no terraces at these sites. The other five sites have more than one step, and hence they have terraces. One unusual case occurs at Mankato, where the river channel has been artificially channelized so that even extreme floods are still confined within the flood control channel.

In order to analyze the results of the normalized water height and surface width from 10-year and 100-year floods, the values on every cross-section of the valley reaches are presented in box plots in Figure 8c. These values correspond to the open and closed symbols in Figure 7. Median values of normalized water surface width at the 10-year and 100-year floods are within the range width/$W_{bf} = 18 \pm 4$ (i.e. the zone enclosed by the long dashed box in Figure 8(c1).

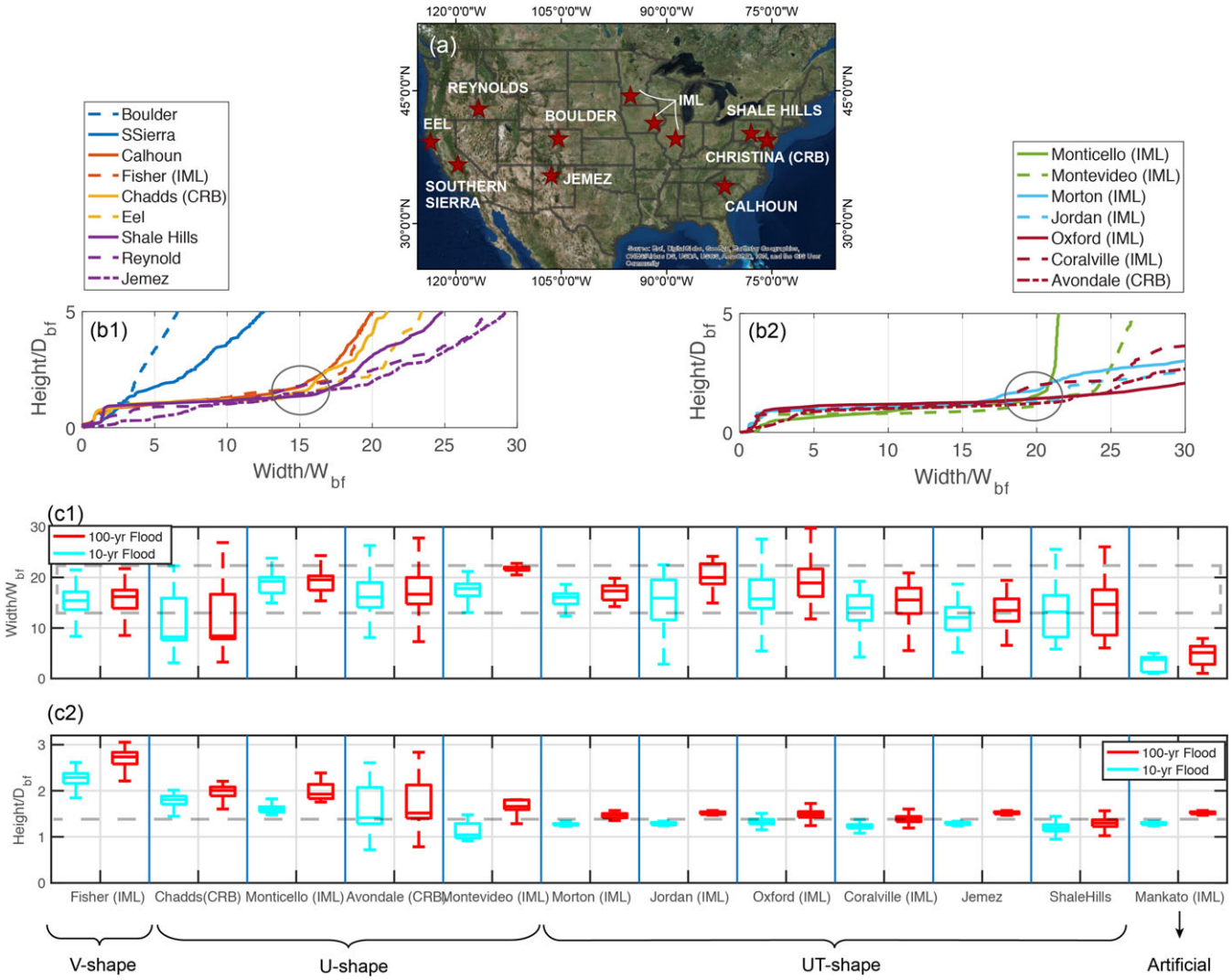

Figure 8. Results of the eight study sites in the US Midwest along with those for other Critical Zone Observatory sites. (a) Locations of CZO sites in the USA. (b) Normalized RVH curves for all of the study sites, which are divided into two groups. The RVH curves in (b1) collapse into a range (width/W_{bf}, height/D_{bf}) $\leq$ (15, 2), while RVH curves in (b2) collapse into a range (width/W_{bf}, height/D_{bf}) $\leq$ (20, 2). (c) Box–whisker plots showing normalized water surface width (c1) and water height (c2) corresponding to the 10-year and 100-year flooding events, respectively. These sites have relatively long discharge records. [Colour figure can be viewed at wileyonlinelibrary.com]

Notably, normalized heights of both the 10-year and 100-year floods progressively decrease from left (V-shape valley) to right (UT-shape valley) in Figure 8(c2). A rough estimate of the normalized water height for flooding zone in UT-shape river valleys is about 1.4.

Discussion

Our approach, which combines the concept of river valley hypsometric (RVH) curves with flood simulation, establishes that the demarcation between floodplains and terraces can be identified from the structure of steps and risers in the RVH curves, which can in turn be obtained from the DEM data. Further, it shows that these transitions may themselves be shaped by floods with 10-year to 100-year recurrences. Simulations of the 10-year and 100-year floods (Figure 7) demonstrate that the water levels are typically confined within the riser (or 'inner walls') between the lowermost and second lowermost steps (low-gradient segments) on the RVH curves. We infer this riser (or 'inner wall') to be the transition between the floodplain and the lowest terrace. Hence one can obtain a first estimate of the maximum area at risk of flooding by locating the first step on a representative RVH curve.

To test the generality of the findings beyond the alluvial valleys of the US Midwest, we expand the analysis to nine other CZO (Critical Zone Observatory) sites (Figure 8a). We plot the RVH curves for all the CZO sites using LiDAR data. Based on the zones of the RVH curves, these sites can be divided into two groups. The RVH curves in Figure 8(b1) loosely collapse into the range (width/W_{bf}, height/D_{bf}) $\leq$ (15, 2), while RVH curves in Figure 8(b2) loosely collapse into the range (width/W_{bf}, height/D_{bf}) $\leq$ (20, 2). River valleys in Figure 8(b2) are more inclined to be in a plain setting, whereas those in Figure 8(b1) are more inclined to be in a mountain setting. Two sites that do not fall into these two ranges are in Boulder and Southern Sierra, whose river valleys are in very steep mountain regions. Flood simulations are conducted at four out of the nine sites: Chadds and Avondale in Christina River Basin, Jemez River Basin and Shale Hills, all of which have long periods of discharge records (see Supporting Information Table S3). The simulation results are shown in Figure 8c along with the IML sites (note that the channel in Mankato is largely expanded for flood control). The modeled water surface widths and heights of 10-year and 100-year floods are

in general correspondence with results for the Midwestern sites (USRB, MRB and CCW) used to develop our method of analysis.

The relationships outlined above suggest that there may exist a quasi-equilibrium condition at which floodplain geometry, as expressed in terms of the width (horizontal span) and depth (distance to the river bottom) is consistently proportional to bankfull width and depth. A likely explanation is that the bankfull discharge, which characterizes the hydraulic geometry and morphodynamics of the main channel (Park, 1977; Rhodes, 1977; Williams, 1978; Knighton, 1998; Dodov, 2004; Li *et al.*, 2014), has a significant impact on floodplain formation itself (Singh, 1972; Ray, 1976; Nanson, 1980; Bridge, 1984; Bown and Kraus, 1987; Belmont, 2011; Iwasaki *et al.*, 2015). It should be recalled in this regard that in alluvial rivers the channel/floodplain complex is a single unit. The floodplain is sculpted by a combination of channel migration and overbank deposition, and channel bankfull depth is defined relative to the adjacent floodplain. River meandering plays an essential role in the formation of floodplains (Lauer and Parker, 2008). The ratio of meander belt width to bankfull width is found from two examples given by Leopold *et al.* (1964) to take the values 10.9 and 18.6, respectively, i.e. close to the range 18 ± 4 found in this work.

The RVH curves reveal that the relation between bankfull channel depth (or width) and floodplain depth (or width) is linear over a range of scales. This result is also consistent with the work done by Dodov and Foufoula-Georgiou (2005). For example, if we assume $W_{\text{floodplain}}/W_{\text{bf}}$ and $H_{\text{floodplain}}/D_{\text{bf}}$ are constant, then the relations between $W_{\text{floodplain}}$ (or $H_{\text{floodplain}}$) and bankfull discharge Q can be expressed in terms of power-law relationships ($\propto kQ_{bf}^{\alpha}$, where k and α are constant parameters). These expressions allow characterization of the floodplain to be brought into the general class of relations for bankfull geometry.

Conclusion

We have introduced the concept of the river valley hypsometric (RVH) curve to make river valley geomorphic features easier to identify and interpret. The statistical interpretation of RVH curves aids in distinguishing features that are not readily seen directly from the DEM data. Our procedure integrates LiDAR topography and numerical modeling to study the relation between flood inundation and geomorphic features for eight sites within three river valleys in the Upper Midwest, namely, MRB (Minnesota River Basin), USRB (Upper Sangamon River Basin) and CCW (Clear Creek Watershed). We found both unique and common features among the eight study sites. Our results indicate that, except in the floodplain of a highly channelized reach of the Minnesota River, (a) the areal extent of the 10-year flood provides a good surrogate for the floodplain itself, and (b) this areal extent increases only modestly at the 100-year flood. The extent of the floodplain can also be identified in terms of the extent of the lowermost step on the RVH curve, which is in range 14–22 times the bankfull width. Normalized water surface widths and heights for both the 10-year or 100-year floods are found to be within a fairly specific range (18 ± 4 and 1.5 ± 0.1, respectively) for what we interpret to be U-shape valleys with terraces (UT-shape). These fairly simple results may be useful in the context of river valley research such as the morphodynamics of floodplain formation and flood risk assessment. We have extended and verified our analysis using nine other sites that cover a more diverse range of geomorphic settings. Our formulation provides a useful tool for the future analysis of other river valleys, and the extraction of generalizations from such analysis. Our results are likely to have some degree of general applicability to rivers in the upper Midwest of North America, as well as rivers in plains in other parts of the world. The separation of floodplains from terraces in a river valley plays an important role in water resource management and flood forecasting and planning.

Acknowledgements— Funding support from National Science Foundation Grants EAR 13-31906 (Intensively Managed Landscapes Critical Zone Observatory – IMLCZO), CBET 12-90445, ACI 12-61582 (Brown Dog) and USGS Powell Center HRT Synthesis Working Group is gratefully acknowledged. We also acknowledge Professor Bruce Rhoads, Professor Alison Anders and Laura Keefer for the insightful discussion on geomorphic processes, particularly in Upper Sangamon River Basin. Thanks to Angela Magnuson for assistance with data collection and flood simulations associated with some CZO sites. The authors declare no conflict of interest.

References

Abaci O, Papanicolaou ANT. 2009. Long-term effects of management practices on water-driven soil erosion in an intense agricultural sub-watershed: monitoring and modelling. *Hydrological Processes* **23**: 2818–2837.

Arthington AH, Pusey BJ. 2003. Flow restoration and protection in Australian rivers. *River Research and Applications* **19**: 377–395.

Belmont P. 2011. Floodplain width adjustments in response to rapid base level fall and knickpoint migration. *Geomorphology* **128**: 92–101.

Belmont P, Gran KB, Schottler SP, Wilcock PR, Day SS, Jennings C, Lauer JW, Viparelli E, Willenbring JK, Engstrom DR, Parker G. 2011. Large shift in source of fine sediment in the upper Mississippi River. *Environmental Science and Technology* **45**: 8804–8810.

Bhowmik NG, Stall JB. Hydraulic geometry and carrying capacity of floodplains, Technical Report Technical Report, University of Illinois at Urbana-Champaign Water Resource Center, 1979.

Bown TM, Kraus MJ. 1987. Integration of channel and floodplain suites. I. Developmental sequence and lateral relations of alluvial paleosols. *Journal of Sedimentary Research* **57**: 587–601.

Bridge JS. 1984. Large-scale facies sequences in alluvial overbank environments. *Journal of Sedimentary Research* **54**: 583–588.

Bridge JS. 2003. *Rivers and Floodplains Forms, Processes, and Sedimentary Record (1st edn)*. Blackwell Science: Oxford.

Bull WB. 1990. Stream-terrace genesis: implications for soil development. *Geomorphology* **3**: 351–367.

Chow VT, Maidment DR, Mays LW. 1988. *Applied Hydrology*. McGraw-Hill: New York.

Cohen KM, Gibbard PL. Global chronostratigraphical correlation table for the last 2.7 million years, Technical Report Technical report. Available: https://quaternary.stratigraphy.org/correlation/POSTERSTRAT_v2011.pdf.20110222-162627 [6 September 2017]., 2016.

Corenblit D, Baas ACW, Bornette G, Darrozes J, Delmotte S, Francis RA, Gurnell AM, Julien F, Naiman RJ, Steiger J. 2011. Feedbacks between geomorphology and biota controlling Earth surface processes and landforms: a review of foundation concepts and current understandings. *Earth-Science Reviews* **106**: 307–331.

Degiorgis M, Gnecco G, Gorni S, Roth G, Sanguineti M, Taramasso AC. 2012. Classifiers for the detection of flood-prone areas using remote sensed elevation data. *Journal of Hydrology* **470–471**: 302–315.

Dodov B. 2004. Generalized hydraulic geometry: derivation based on a multiscaling formalism. *Water Resources Research* **40**: 1–22.

Dodov B, Foufoula-Georgiou E. 2005. Fluvial processes and streamflow variability: interplay in the scale-frequency continuum and implications for scaling. *Water Resources Research* **41**: 1–18.

Eash DA, Barnes KK, Veilleux AG. Methods for estimating annual exceedance-probability discharges for streams in Iowa, based on data through water year 2010, Technical Report Technical report USGS, Reston, VA, 2013.

Fan J. 2016. International Stratigraphic Chart.

Foufoula-Georgiou E, Takbiri Z, Czuba JA, Schwenk J. 2015. The change of nature and the nature of change in agricultural landscapes: hydrologic regime shifts modulate ecological transitions. *Water Resources Research* **51**: 6649–6671.

Gran KB, Finnegan N, Johnson AL, Belmont P, Wittkop C, Rittenour T. 2013. Landscape evolution, valley excavation, and terrace development following abrupt postglacial base-level fall. *Bulletin of the Geological Society of America* **125**: 1851–1864.

Grimaldi S, Petroselli A, Arcangeletti E, Nardi F. 2013. Flood mapping in ungauged basins using fully continuous hydrologic–hydraulic modeling. *Journal of Hydrology* **487**: 39–47.

Hancock G, Anderson RS. 2002. Numerical modelling of fluvial strath terrace formation in response to oscillating climate. *Bulletin of the Geological Society of America* **114**: 1131–1142.

Harvey J, Gooseff M. 2015. Consequences from bedforms to basins. *Water Resources Research* **51**: 6893–6922.

Hopkins AJ, Snyder NP. 2016. Performance evaluation of three DEM-based fluvial terrace mapping methods. *Earth Surface Processes and Landforms* **41**: 1144–1152.

Iwasaki T, Nabi M, Shimizu Y, Kimura I. 2014. Computational modeling of 137Cs contaminant transfer associated with sediment transport in Abukuma River. *Journal of Environmental Radioactivity* **139**: 416–426.

Iwasaki T, Shimizu Y, Kimura I. 2015. Numerical simulation of bar and bank erosion in a vegetated floodplain: a case study in the Otofuke River. *Advances in Water Resources* **93**: 118–134.

Jennings CE, Johnson MD. 2011. *The Quaternary of Minnesota*, 1st edn, Vol. 15. Elsevier: Amsterdam.

Killey MM. IllinoisâĂŹ Ice Age legacy, Technical Report Technical report, Illinois State Geological Survey Champaign, IL, 2007.

Knighton D. 1998. *Fluvial Forms and Processes: A New Perspective*. Routledge: London.

Kumar P. 2011. Typology of hydrologic predictability. *Water Resources Research* **47**: 1–9.

Lauer JW, Parker G. 2008. Modeling framework for sediment deposition, storage, and evacuation in the floodplain of a meandering river: application to the Clark Fork River, Montana. *Water Resources Research* **44**: 1–16.

Leopold LB, Maddock T Jr. 1953. *The hydraulic geometry of stream channels and some physiographic implications*. Geological Survey Professional Paper 252: USGS Reston, VA.

Leopold LB, Wolman LG, Miller JP. 1964. *Fluvial Processes in Geomorphology (1st edn)*. Freeman: San Francisco, CA.

Li C. 2014. *Modeling the transport of sand and mud in the Minnesota River*. University of Illinois at Urbana-Champaign: PhD thesis.

Li C, Czapiga MJ, Eke EC, Viparelli E, Parker G. 2014. Variable Shields number model for river bankfull geometry: bankfull shear velocity is viscosity-dependent but grain size-independent. *Journal of Hydraulic Research* **1686**: 1–13.

Limaye ABS, Lamb MP. 2014. Numerical simulations of bedrock valley evolution by meandering rivers with variable bank material. *Journal of Geophysical Research: Earth Surface* **119**: 927–950.

Lorenz DL, Sanocki CA, Kocian MJ. 2010. *Techniques for estimating the magnitude and frequency of peak flows on small streams in Minnesota based on data through water year 2005*: USGS Reston, VA.

Mickelson DM, Colgan PM. 2003. The southern Laurentide Ice Sheet. *Developments in Quaternary Science* **1**: 1–16.

Nanson GC. 1980. Point bar and floodplain formation of the meandering Beatton River, northeastern British Columbia, Canada. *Sedimentology* **27**: 3–29.

Nanson GC, Croke JC. 1992. A genetic classification of floodplains. *Geomorphology* **4**: 459–486.

Nelson JM, Shimizu Y, Abe T, Asahi K, Gamou M, Inoue T, Iwasaki T, Kakinuma T, Kawamura S, Kimura I, Kyuka T, McDonald RR, Nabi M, Nakatsugawa M, Simões FR, Takebayashi H, Watanabe Y. 2016. The international river interface cooperative: public domain flow and morphodynamics software for education and applications. *Advances in Water Resources* **93**: 62–74.

Noman NS, Nelson EJ, Zundel AK. 2001. Review of automated floodplain delination from digital terrain models. *Journal of Water Resources Planning and Management* **127**: 394–402.

Opperman JJ, Galloway GE, Fargione J, Mount JF, Richter BD, Secchi S. 2009. Sustainable floodplains through large-scale reconnection to rivers. *Science* **326**: 1487–1488.

Park CC. 1977. World-wide variations in hydraulic geometry exponents of stream channels: an analysis and some observations. *Journal of Hydrology* **39**: 199–202.

Passalacqua P, Belmont P, Staley DM, Simley JD, Arrowsmith JR, Bode CA, Crosby C, DeLong SB, Glenn NF, Kelly SA, Lague D, Sangireddy H, Schaffrath K, Tarboton DG, Wasklewicz T, Wheaton JM. 2015. Analyzing high resolution topography for advancing the understanding of mass and energy transfer through landscapes: a review. *Earth-Science Reviews* **148**: 174–193.

Patterson C, Hansel D, Mickelson D, Quade D, Bettis E, Colgan P, McKay E, Stumpf A. 2003. Contrasting glacial landscapes created by ice lobes of the southern Laurentide Ice Sheet. In *Quaternary Geology of the United States*, Easterbrook D J (ed), Technical report, Desert Research Institute: Reno, NV.

Pazzaglia FJ. 2013. Fluvial terraces. *Treatise on Geomorphology* **9**: 379–412.

Pazzaglia FJ, Gardner TW. 1993. Fluvial terraces of the lower Susquehanna River. *Geomorphology* **8**: 83–113.

Ray PK. 1976. Structure and sedimentological history of the overbank deposits of a Mississippi River point bar. *Journal of Sedimentary Research* **46**: 788–801.

Rayburn AP, Schulte LA. 2009. Landscape change in an agricultural watershed in the U.S. Midwest. *Landscape and Urban Planning* **93**: 132–141.

Rhoads BL, Lewis QW, Andresen W. 2016. Historical changes in channel network extent and channel planform in an intensively managed landscape: natural versus human-induced effects. *Geomorphology* **252**: 17–31.

Rhodes DD. 1977. The b-f-m diagram: graphical representation and interpretation of at-a-station hydraulic geometry. *American Journal of Science* **277**: 73–96.

Rovey CW, Balco G. 2015. Paleoclimatic interpretations of buried paleosols within the pre-Illinoian till sequence in northern Missouri, USA. *Palaeogeography Palaeoclimatology Palaeoecology* **417**: 44–56.

Rovey CW, McLouth T. 2015. A near synthesis of pre-Illinoian till stratigraphy in the central United States: Iowa, Nebraska and Missouri. *Quaternary Science Reviews* **126**: 96–111.

Schumm SA. 2005. *River Variability and Complexity (1st edn)*. Cambridge University Press: Cambridge, UK.

Singh IB. 1972. On the bedding in the natural-levee and the point-bar deposits of the Gomti river, Uttar Pradesh, India. *Sedimentary Geology* **7**: 309–317.

Soller D, Packard P, Garrity C. Database for USGS Map I-1970: map showing the thickness and character of Quaternary sediments in the glaciated United States east of the Rocky Mountains, Technical Report Technical report, USGS Data Series 656 USGS Reston, VA, 2012.

Soong DT, Ishii AL, Sharpe JB, Avery CF. Estimating flood-peak discharge magnitudes and frequencies for rural streams in Illinois, Technical Report Technical report USGS Reston, VA, 2004.

Stout JC, Belmont P. 2014. TerEx Toolbox for semi-automated selection of fluvial terrace and floodplain features from lidar. *Earth Surface Processes and Landforms* **39**: 569–580.

Strahler AN. 1952. Hypsometric analysis of erosional topography. *Bulletin of the Geological Society of America* **63**: 1117–1142.

Wheaton JM, Fryirs KA, Brierley G, Bangen SG, Bouwes N, Brien GO. 2015. Geomorphic mapping and taxonomy of fluvial landforms. *Geomorphology* **248**: 273–295.

Wilcock P. Synthesis report for Minnesota River sediment colloquium, Technical Report Technical report, MPCA, 2009.

Williams GP. 1978. Bankfull discharge of rivers. *Water Resources Research* **14**: 1141–1154.

Wilson CG, Papanicolaou ANT, Abaci O. 2009. SOM dynamics and erosion in an agricultural test field of the Clear Creek, IA watershed. *Hydrology and Earth System Sciences* **6**: 1581–1619.

Wongsa S. 2014. Simulation of Thailand Flood 2011. *International Journal of Engineering and Technology* **6**: 452–458.

Wyrick J, Senter A, Pasternack G. 2014. Revealing the natural complexity of fluvial morphology through 2D hydrodynamic delineation of river landforms. *Geomorphology* **210**: 14–22.

Supporting Information

Additional supporting information may be found online in the supporting information tab for this article.